Synergy effect between layer double hydroxide (LDH) and EDDS for corrosion inhibition of carbon steel

Sabrina Marcelin, Gata Joseph Ayemi, Sandrine Therias, Leroux Fabrice, Bernard Normand

Synergy effect between layer double hydroxide (LDH) and EDDS for corrosion inhibition of carbon steel

G. J. Ayemi[a], S. Marcelin[a*], S. Thérias[b], F. Leroux[b], B. Normand[a]

[a] Université de Lyon, INSA Lyon, MATEIS UMR CNRS, F-69621 Villeurbanne cedex, France

[b] Université Clermont-Auvergne-CNRS-UMR 6296, ICCF F-63178 Aubière, France

Abstract

Ethylenediamine-N,N'-disuccinate (EDDS) is successfully intercalated between layered double hydroxide (LDH) sheets leading to hybrid assembly $[Zn_2Al(OH)_6]^+ [EDDS]^{4-}_{0.25} 2H_2O$ (LDH-$EDDS^{4-}$). The electrochemical behaviour of the carbon steel carried out in a neutral and aerated sodium chloride solution shows the surface reactivity of carbon steel is significantly decreased in presence of functionalized LDH-$EDDS^{4-}$. To elucidate the inhibition mechanism provided by the hybrid assembly LDH-$EDDS^{4-}$, each part constituting the funtionalized LDH is studied alone (Zn^{2+}, Al^{3+} or $EDDS^{4-}$) or in combination. A synergy effect between Zn^{2+} cations and $EDDS^{4-}$ anions is highlighted by anodic polarization and electrochemical impedance. In addition SEM and visual observations confirm the efficiency provided by the hybrid LDH-$EDDS^{4-}$ to protect carbon steel surface from corrosion.

Keywords : Carbon steel, LDH, EDDS, Corrosion inhibition, EIS

* Corresponding author : sabrina.marcelin@insa-lyon.fr

1. Introduction

Organic coatings, inhibitors, and cathodic protection among others have been employed for corrosion protection of carbon steel (Ekott et al., 2012; Nguyen et al; 2018; Obot and Anyakwo, 2017;). Against environment, organic coatings are chosen for their barrier effect to protect the substrate. However, most organic coatings are prone to water uptake (Garden and Pethrick, 2017; Morsh et al., 2015) which can lead to the substrate corrosion. To compensate this situation**,** inhibitors can be added in the polymer matrix (Stimpfling et al., 2012) to act with metallic cations from substrate to block the cathodic or anodic or both reactions at the metal/electrolyte interface. Therefore, special attention must be paid to the compatibility between the inhibitors and the organic matrix to ensure the protective character of the new protection system. Smart-coatings are developed to provide "active corrosion protection" for metal substrates (Cao et al., 2022; Zheludkevich et al., 2012), which confer the so-called "smart properties" of the coatings. A strategy widely used is to develop smart-coating is by incorporating a "guest host" assembly as a corrosion inhibitor reservoir with an ability to respond to an external stimulus (Zhang et al., 2019).

Among these reservoirs, LDH as a promising reservoir for corrosion inhibitors had gained more attention. This is due to its particular chemical structure, which combines tunability and versatility in terms of: - a wide range of combinations between divalent and trivalent cations (Zn-Al, Mg-Al, Ni-Fe, Ni-Al, etc.), - a high anion exchange capacity (release and uptake) and, - a sensitive response to specific stimulus (exchange through mass action law, pH,…) (Bakhtaoui et al., 2021; Deip et al., 2020; Peng et al.; 2020; Truc et al., 2019).

Layered double hydroxides, named also hydrotalcite or anionic clay materials, are lamellar structures. They are composed of positively-charged hydroxide layers of mixed metallic cations,with negatively-charged exchangeable anions and water molecules present within their interlayer gallery spacing. They have a similar structure to brucite ($Mg(OH)_2$) compounds. Partial substitution between divalent by trivalent cations is charge-balanced by the anions as illustrated by (Alibakhshi et al., 2017). They have a general formula $\left[M^{2+}_{(1-x)}M^{3+}_{x}(OH)_2\right]^{+}\left[A_{x/n}\right]^{n-}.yH_2O$, where M^{2+} and M^{3+} are the divalent (Zn^{2+}, Mg^{2+}, Ca^{2+}, Ni^{2+}, Fe^{2+}, Co^{2+}, Cd^{2+}, etc) and trivalent (Al^{3+}, Cr^{3+}, Fe^{3+}, Co^{3+}, etc) metal cations,

respectively, A^{n-} is the exchangeable charge-balancing anion with a valence of n which is located between the interlayer spacing, *x* is the ratio of $[M^{3+}]/([M^{3+}] + [M^{2+}])$ which is usually between 0.25 $\leq x \leq 0.33$ range and *y* is number of water molecule (Liu et al., 2019).

Inhibitor-loaded LDH is an on-demand releasing system with the aim of delivering an inhibitive species to a targeted corrosion sites of the metallic substrate when exposed to electrolyte (Nguyen et al., 2018; Stimpfling et al., 2012). The inhibitor releasing from LDH is coupled with the simultaneous capturing of chloride ions from electrolyte environment. Therefore, LDH play a double inhibition role as a reservoir for corrosion inhibitor and also as a scavenger to trap aggressive species (Cao et al., 2021; Hang et al. 2012; Leal et al., 2020). The following organic inhibitors: ethylenediaminetetraacetic acid (EDTA) (Stimpfling et al., 2013), Benzothiazolylthio-succinic acid (BTSA) (Hang et al., 2012; Hang et al., 2015; Nguyen et al., 2016), benzotriazole (BTA) (Deip et al., 2020; ; Rodriguez et al., 2020; Seniski et al., 2020; Serdechnova et al., 2016; Truc et al., 2019), 8-hydroxyquinoline (8-HQ) (Truc et al., 2019), Indole-3 butyric acid (IBA) (Hang et al., 2010; Truc et al., 2008) intercalated into their respective reservoir had been studied to hinder carbon steel corrosion. That is, the inhibitor released from LDH migrates to the metallic substrate, are adsorbed or form a protective barrier or oxide film which could block either or both the anodic or cathodic reactions of corrosion (Leal et al., 2020, Sui et al.,2021; Truc et al., 2019). Most of the studies were focussed only on the releasing ability of LDH but had neglected the solubility of LDH scalfold in the electrolyte solution. There are limited studies on the contribution of each individual components of LDHs and/or synergistic effect between their component on carbon steel corrosion inhibition.

As mentioned earlier, EDTA acts as a corrosion inhibitor for carbon steel. However, it is harmful and should be replaced by another compound. Biodegradable ethylenediamine-N,N′-disuccinic acid (EDDS) has a chemical structure close to the EDTA (Metsärine et al., 2011), as chelating agent able to hexadentate thus, it should be a good candidate to protect carbon steel against corrosion. This work is an opportunity to fill this knowledge gap and also to study the efficiency of EDDS, little studied as free or intercalated inhibitor into LDH. This work focusses on the synthesis and characterization of intrinsic properties of Zn_2Al LDH intercalated with organic anion of ethylenediamine-N,N′-disuccinate solution ($EDDS^{4-}$) through co-precipitation process.

The crystal structure of the LDH-$EDDS^{4-}$ was studied using X-ray diffraction (XRD). Scanning Electron Microscopy (SEM) was employed to study the morphology of LDH power and protective layer formed at the surface of the carbon steel substrate after immersion in chloride solution. ICP-OES was used to measure the solubility of zinc and aluminium hydroxides layers. To possibly elucidate the inhibitive mechanism from the LDH-$EDDS^{4-}$, the inhibitive effect of each element which includes Zn^{2+}, Al^{3+} and $EDDS^{4-}$ and the synergistic inhibition effect of these components in 0.1M sodium chloride solution was studied by anodic polarisation curves and by electrochemical impedance spectroscopy performed at corrosion potential to evaluate their efficiency as carbon steel corrosion inhibitor.

2. Experimental

2.1. Materials

Zinc nitrate hexahydrate $Zn(NO_3)_2.6H_2O$ (98 extra, Acros Organics), aluminum nitrate nonahydrate $Al(NO_3)_3.9H_2O$ (99%, Acros Organics), sodium nitrate $NaNO_3$ (Prolabo), sodium hydroxide NaOH (> 98%, Sigma Aldrich), 35% in water ethylenediamine-N,N′-disuccinic acid trisodium salt solution $C_{10}H_{13}N_2Na_3O_8$ (pKa = 2.4, Sigma Aldrich), and sodium chloride (Sigma Aldrich). The chemical structure of EDDS is shown in Figure 1.

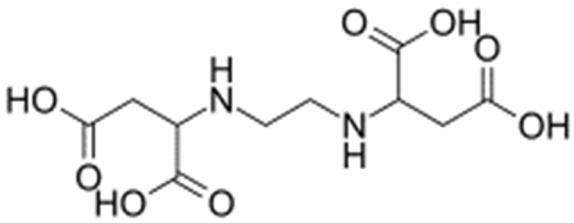

Figure 1: Molecular structure of ethylenediamine-N,N'-disuccinic acid.

To evaluate the corrosion inhibition efficiency of LDH-$EDDS^{4-}$, a cylindrical XC38 carbon steel rod (C = 0.32-0.39, S ≤ 0.035, Mn = 0.5.-0.80, P ≤ 0.035, Si = 0.40 max, Fe to 100, in wt.%) covered

with adhesive lined heat-shrinkable tube baring only a disk of 1 cm² cross section was used as working electrode. Before each experiment, the sample was mechanically polished with SiC abrasive papers down to 2400 grade, then rinsed with ethanol in ultrasonic bath before air drying.

2.2. Synthesis of $[Zn_2Al(OH)_6]^+[EDDS^{4-}]_{0.25}.2H_2O$ layer double hydroxides (LDH-$EDDS^{4-}$)

The zinc-aluminum LDH intercalated with the anions of ethylenediamine-N,N′-disuccinic acid trisodium salt ($[Zn_2Al(OH)_6]^+[EDDS^{4-}]_{0.25}.2H_2O$) was prepared at room temperature by direct co-precipitation route. The synthesis mole ratio of 2:1 for Zn:Al was chosen to obtain a stable LDH-$EDDS^{4-}$. 300 mL of a solution containing a mixture 0.028 mol of $Zn(NO_3)_2.6H_2O$ and 0.014 mol of $Al(NO_3)_3.9H_2O$, was gradually added in a dropwise manner at a constant flowrate of 2.5 mL/min to 300 mL solution containing 0.017 mol of trisodium EDDS under slow and then vigorous stirring for 2 hours. Simultaneously, the synthesis pH value of the mixed solutions was kept close to 9 to optimize the co-precipitation of both Al^{3+} and Zn^{2+} to form LDH platelets. Thus, the achieved synthesis pH was 8.7±0.1 by controllable dropwise addition of 300 mL solution containing 0.20 mol of NaOH at the flow rate of 1 mL/min during the co-precipitation reaction (Theiss et al., 2016). To exclude carbonate anions from the LDH, the experiment was carried out under nitrogen atmosphere. The white precipitate suspension formed at the end of the experiment was centrifuged at 4500 rpm for about 10 minutes to obtained the slurry of Zn_2Al-EDDS LDH particles. The slurry was washed three times with deionized water to removed unreacted elements and part of the sample was dried in an oven at 50°C for 24 hours. Deionized water was used in the rinsing and preparation of aqueous solution procedures to ensure proper purity of the LDHs synthetized.

2.3. Analytical characterizations

X-ray diffraction measurements were performed with a Bruker diffractometer (Cu K_α, λ=1.5406Å radiation source, Lynx eye detection, 2θ scan range of 5° - 90° in 0.02° scan steps and 184 s count time per step) to characterize the intercalation of EDDS, the crystal structure of LDHs, and to highlight the anion exchange between $EDDS^{4-}$ and Cl^- providing from the electrolyte. The sample for

studying the anion exchange between $EDDS^{4-}$ and Cl^- in electrolyte solution was obtained in a powder form, after 72 h of magnetic stirring and dehydration of the neutral chloride solution containing the inhibitive species (0.1 M NaCl + 15 g/L LDH-$EDDS^{4-}$).

SEM observations were carried out using a VEGA3 TESCAN and a Zeiss Supra 55VP apparatus to observed the morphologies of the LDH-$EDDS^{4-}$ and the surface state of the carbon steel after immersion in different electrolytes, respectively.

2.4. Quantification of hydroxide layers dissolution by ICP-OES

The solubility of Zn_2Al-EDDS LDH scaffold in 0.1 M NaCl was studied by an inductively coupled plasma-optical emission spectroscopy (ICP-OES). For this purpose, 150 mg of LDH-$EDDS^{4-}$ slurry was added to 10 mL of 0.1M NaCl solution and then magnetically stirred at 300 rpm for 1 h. The mixture was centrifuged at 4500 rpm for 45 mins to obtain a clear extracted solution. The same procedure was repeated up to 72 h. For each extracted solution, the pH was measured using a standard pH meter PHM210 by radiometer analytical. The concentrations of Zn^{2+} and Al^{3+} metallic cations released from the LDH were measured using ICP-OES modelled as iCAP 7400 by thermofischer scientific. The analysis was performed in an axial and radial mode with the glass expansion nebulizer at 0.5 mL/min argon (standard ICP-AES conditions).

2.5. Electrochemical characterizations

To evaluate the inhibitive effect of the Zn_2Al-EDDS LDH on carbon steel corrosion, a standard three-electrodes set-up was used. It was constituted by a saturated calomel electrode as the reference electrode and a cylindrical platinum grid as the counter electrode. The working electrode was a rotating disk electrode (RDE) with an exposed disk area of 1 cm^2 of the bare carbon steel. The speed of electrode rotation was fixed at 200 rpm. The volume of the electrochemical cell was 100 mL.

The blank electrolyte solution was constituted by 0.1M NaCl solution (pH = 5.8). To investigate the inhibition mechanism, the following inhibitive component were added to the neutral blank chloride

solution: 0.02 M $Zn(OH)_2$, 0.01 M $Al(OH)_3$, 0.01 M EDDS, either alone, or mixed, and LDH-$EDDS^{4-}$ slurry (5 g/L and 15 g/L). The concentrations of the individual component were chosen with respect to the synthesis molar ratio. For each electrolyte, a volume of 100 mL was prepared by magnetic stirring for 72 hours to obtain a clear extract solution, and the pH of the electrolyte solution was measured before carbon steel electrode immersion.

The electrochemical measurements were carried out in a systematic route and were performed using a Biologic SP-300 potentiostat, at room temperature and under a faraday cage. All electrochemical impedance spectroscopy (EIS) measurements were performed using the last defined solution to ensure and control the coumpounds releasing. After 24 hours of immersion in the last solution, EIS was performed at corrosion potential, using a 10 mV RMS amplitude sinusoïdal perturbation, between 10^5 Hz and 3 mHz and with 8 points per decade. Anodic polarization curves were recorded between from -50 mV vs OCP to +0 V/ECS with a scan rate of 1 mV/s. All measurements were repeated at least three times to ensure the reproducibility. More also, after immersion at the corrosion potential, the surfaces of the carbon steel was observed at macro- and microscopic (by SEM, as earlier mentioned) scale.

3. Results and discussion

3.1. Characterization of LDH-$EDDS^{4-}$

From the SEM images, the particles of LDH-$EDDS^{4-}$ exhibited stacked of agglomerated platelet-like morphology which is typical of layered double hydroxides (Rodriguez et al.,2020). This morphology could be attributed to the nucleation and crystal growth of the LDH particles as a function of the pH value. The observed agglomeration could be due to the initial stages of sheets growth. LDHs are best crystallized at high pH (Alibakhshi et al., 2020; Panda et al., 2011). The sample has the typical plate-like morphology of LDH. The LDH particule size is varying and is of the order of a few micrometers.

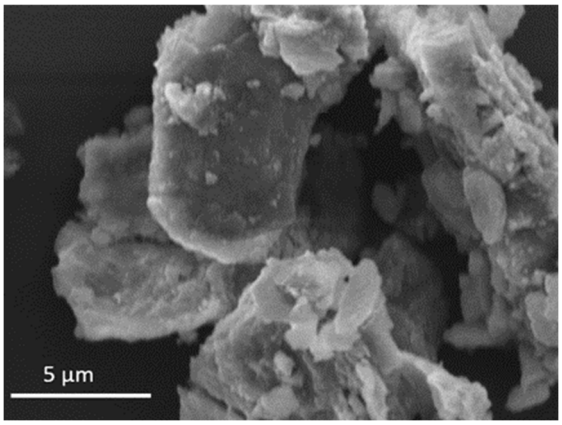

Figure 2: SEM micrograph obtained for synthetized LDH-$EDDS^{4-}$.

The recorded XRD pattern of the synthesized LDH-$EDDS^{4-}$ powders is presented in Figure 3 and shows diffraction peaks at 2θ angles of 6.33°, 12.78°, 19.16°, 34.40° and 61.07°, corresponding to the reflection by (003), (006), (009), (012) and (110) planes of the LDH crystal structure, respectively. The pattern exhibits nearly symmetric diffraction peaks which suggest that, the synthesized powder is monophasic. The presence of a sharp diffraction reflection peak at (003) confirmed the accomodation of EDDS anion into the interlayer galleries of LDH host (Cao et al., 2017; Serdechnova et al., 2016; Stimpfling et al., 2013). The characteristic diffraction reflections corresponding to $R\bar{3}m$ (space group) rhombohedral symmetry were indexed to a hexagonal lattice, generally used to describe LDH crystal structures (Serdechnova et al., 2016; Stimpfling et al., 2013). The anions size and the staking direction of the LDH crystal structure, determine the basal spacing of the hydroxide layers (Chhetri et al., 2019; Serdechnova et al., 2016; Wang and Zhang, 2011). Therefore, using Bragg's law (eq. 1), the basal spacing (*d*) was calculated from the most intense reflection (003) position) (Li et al., 2018; Mei et al., 2019). The $d_{(hkl)}$ values for the diffraction positions (003), (006), and (009) were estimated to be 1.382 nm, 0.691 nm and 0.461 nm respectively, close to that reported for EDTA with 1.462 nm (Stimpfling et al. 2013), signifying that the Zn_2Al-EDDS LDH has a proper stacking direction order and possess a typical brucite layers structure since d(003)= 2d(006) =3d(009) (Ennadi et al., 2000; Stimpfling et al., 2013). Equation 2, was used to determine the gallery height (*h*) of the LDH by subtracting the cationic inorganic layer thickness (t = 0.471 nm = brucite layer) from the ($d_{(003)}$) value (Stimpfling et al., 2012, Stimpfling et al., 2013). By using equations 3 and 4, the lattice parameters (*a*, *c*) were estimated from

the diffraction reflections (110) and (003), respectively (Jaber et al., 2020; Stimpfling et al., 2013; Zhou et al., 2017). The lattice parameter *c*, depends on both the charge and size of the anions (Ennadi et al., 2000; Serdechnova et al., 2016). The lattice as well as other parameters that characterized crystal structure of the synthesized Zn_2Al-EDDS LDH are listed in Table 1.

$$d = \frac{n\lambda}{2\sin\theta} \quad \text{(eq. 1)}$$

$$h = d - t \quad \text{(eq. 2)}$$

$$a = 2d_{(110)} \quad \text{(eq. 3)}$$

$$c = 3d_{(003)} \quad \text{(eq. 4)}$$

Where, d, λ, t, h and θ are the interlayers basal spacing, wavelength of the incident X-ray beam, layers thickness, gallery height and diffraction angle between the incident X-ray and the reflection crystal plane, in nm and degrees, respectively. The parameter n is a constant representing the reflection order, it is usually taken to be 1.

Figure 3 shows the XRD pattern for LDH-$EDDS^{4-}$ after exposure to the NaCl solution. Sharp diffraction peaks observed at 2θ angle of 27.4°, 31.7°, 45.5°, 56.5°, 66.2°, 75.3° and 84.1° are ascribed to NaCl structure. The harmonic diffraction peaks of EDDS LDH are shifted to higher 2 θ values. The peak (003) initially observed at 2θ = 6.4° is shifted to 2 θ = 11.8° giving a basal spacing of d = 0.75 nm, while (006) observed at 2θ = 12.8° is shifted 2θ = 22.9°. After contacting with NaCl, the LDH structure is then modified with a smaller basal spacing of 0.75 nm, value that is similar to chloride LDH reported in the literature (Ennadi *et al.*, 2000). This result suggests the replacement of EDDS anion by chloride anion thereby validates the anion-exchange ability of functionalized LDH. Interestingly it shows that even multiple tethered molecule such as EDDS with its four carboxylate functions, two on each inner-side, is easily released out of LDH host, thanks to a mass action law favoring the uptake of chloride anions.

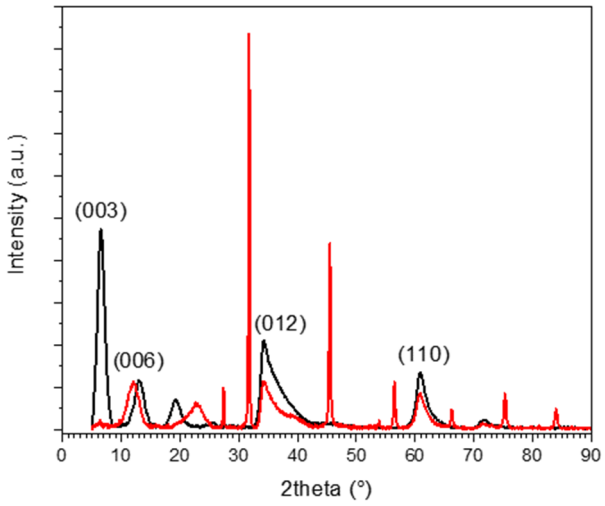

Figure 3: XRD patterns for LDHs containing EDDS before (in black) and after exposure (in red) to the neutral chloride solution.

Table 1: Basal spacing (*d*), gallery height (*h*) and lattice parameters (*a*, *c*) obtained from Zn_2Al LDH intercalated with EDDS anion.

	d (nm)	*h* (nm)	*a* (nm)	*c* (nm)
Zn_2Al-EDDS LDH	1.382	0.911	0.303	4.146

It is generally reported that LDHs releases anions from their interlayer space through ion-exchange mechanism, few studies investigate the release of the cations composing the sheets. For this purpose, ICP-OES analysis were performed to determine the content of divalent and trivalent metallic cations released from Zn_2Al-EDDS LDH. Table 2 reports the concentrations for Zn^{2+} and Al^{3+} as a function of magnetic stirring time in the 0.1M NaCl solution. The pH of all extracted solutions was constant during time and close to the neutrality. The results reveal the presence of zinc and aluminium cations with a significant difference in concentrations (about 42 mg/L and about 0.5 mg/L for Zn^{2+} and Al^{3+}, respectively for the solution extracted after 72 h of stirring) that needs to be further quantified and compared to the initial quantity. Table 3 reports the ratio of dissolved cation/initial quantity for Zn^{2+} and Al^{3+}, in weight percent, calculated from the amount of initial LDH structure concerned by the dissolution (150 mg of LDH-EDDS in 10 mL of NaCl solution). The cation concentration measured in solution after the longest time of 72h leads to less than 1% by mass of the initial cation quantity of LDH powder.

This explains that it is not significant enough to affect the XRD pattern. Moreover, the dissolved amount is not enough to de-stabilize LDH sheet structure. From Table 2, it is interesting to note that, Zn^{2+} cations are no longer released after 24 h. On the other hand, Al^{3+} cations are not significantly dissolved. Such pronounced difference in dissolution between cations results in LDH material with a ratio Al^{3+}/Zn^{2+} slightly higher than initially, so leaving LDH structure prone to trap even more chlorine anions.

Table 2: Concentrations of Zn^{2+} and Al^{3+} released during time from Zn_2Al-EDDS LDH extracted solutions in exposure in 0.1M NaCl solution

Magnetic Stirring Time (h)	Zn^{2+} (mg/L)	Al^{3+} (mg/L)	pH at 25°C
1	21.1	0.13	6.9
24	49.20	0.14	6.8
72	41.50	0.50	6.7

Table 3: Mole and weight of LDH-EDDS, Zn^{2+} and Al^{3+} initially presents in the 150 mg of LDH-EDDS and ratio between dissolved cation and initial quantity of cation after 72h of magnetic stirring in 10 mL of 0.1M NaCl solution (from Table 2).

Chemical species	Mole (n)	Weight (mg)	ratio [dissolved cation/initial quantity] (wt. %)
LDH-EDDS	$0.407\ 10^{-3}$	150	-
Zn^{2+}	$0.814\ 10^{-3}$	53	0.78
Al^{3+}	$0.407\ 10^{-3}$	11	0.045

Therefore, the results validate the fact that, functionalized LDHs do not only release $EDDS^{4-}$ anions (and trap chloride anions), but also a part of zinc cations. These two components could play a role in the inhibition of the carbon steel corrosion, which is investigated in the next section.

3.2. Electrochemical behavior of carbon steel in the presence of LDH-EDDS^{4-} and the role of each components

Polarisation curves obtained for the carbon steel after 24 h of immersion in the chloride solution and the solution containing the synthetized LDH-EDDS^{4-} at two different concentrations (5 and 15 g/L) are presented in Figure 4. In the presence of LDH-EDDS^{4-}, the corrosion potential shifts towards more anodic value meanwhile a decrease of the anodic current density values are observed. This trend is emphasized when the functionalized LDH concentration increases. Deip *et al.* observed similar trends from commercially produced Zn-Al layered double hydroxide intercalated with BTA for carbon steel immersed in 35 wt. % NaCl electrolyte (Deip. et al., 2020). For the highest concentration of LDH-EDDS^{4-}, the anodic domain is characterized by a pseudo-plateau between -0.5 and -0.3 V/ECS and the anodic current density is about 10^{-2} A/cm^2. From these observations, it can be concluded that the shift in corrosion potential and the decrease in anodic current densities is due either to the synthesized LDH-EDDS^{4-} (leading to the presence of EDD^{4-} and Zn^{2+} in the electrolyte) or to the decrease in chloride concentration, or both.

To validate this fact and discriminate the effect of zinc cations and EDDS^{4-} anions, anodic polarisation curves are performed in the presence of zinc hydroxide (0.02 M) and ethylenediamine-N,N'-disuccinic acid (0.01 M) with the same protocol as previous ones and are shown in Figure 5. In the presence of EDDS, the corrosion potential is shifted to more anodic value (-0.55 V/ECS by comparison with the chloride (blank) solution where the corrosion potential value is about -0.70 V/ECS). The anodic current densities are lower than for the reference result. The shape of the polarisation curve in the anodic domain is similar to that of the anodic curve presented in Figure 4, for the higest concentration of LDH.

In the presence of zinc hydroxide alone, the electrochemical behavior of the carbon steel is different with a shift to more anodic value of the corrosion potential, a more decrease in the anodic current density. Moreover, the shape of the polarization curve exhibits a pseudo-passive plateau before a significant increase of the current densities at around -0.35 V/ECS. It should be underlined that the pH in the presence of EDDS is more basic than in the presence of $Zn(OH)_2$. For comparison, the polarisation curve obtained in presence of aluminium hydroxide (0.01 M) is similar to the curve obtained in the blank

chloride solution. This last result shows that Al^{3+} cations do not modify the reactivity of the carbon steel and thus, the weak released content from LDH does not act in inhibiting the corrosion for carbon steel. In presence of Zn^{2+} cations and $EDDS^{4-}$ anions in the neutral chloride solution (0.1 M), the anodic polarisation curve (Fig. 5) is different than before (Fig. 4) with a sharp decrease of the anodic current densities and a plateau defined in a large potential domain where the anodic current density is closed to 10^{-5} A/cm² followed by an increase in current density at -0.15 V/ECS, corresponding to a pitting potential. This result clearly shows the synergy effect between zinc cation and EDDS to inhibit carbon steel corrosion. The polarization curves obtained in presence of Al^{3+} alone (Fig. 5) or in mixture with EDDS and zinc hydroxide (Fig. 6) confirms its spectator role. Thus the inhibitive properties of the hybrid Zn_2Al-$EDDS^{4-}$ come from the decrease of chloride content by trapping and/or from the synergy between zinc cations and $EDDS^{4-}$ anions. It must be underlined that Al^{3+} doesn't play a role on the corrosion inhibition of carbon steel but is needed to stabilize the host structure.

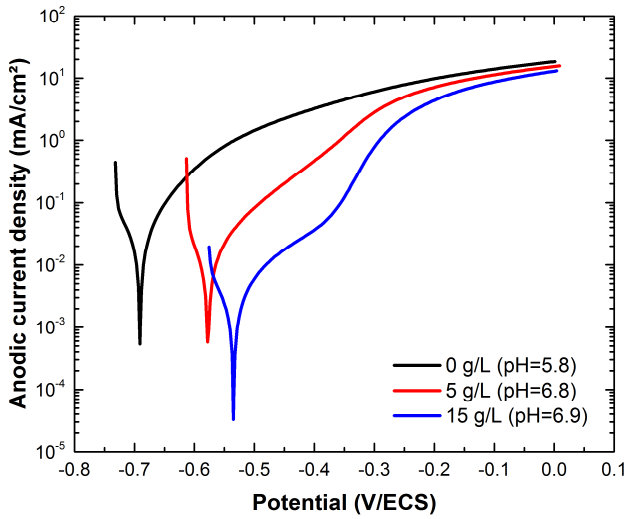

Figure 4: Anodic polarization curves obtained for the carbon steel (RDE rotation speed = 200 rpm) after 24 h in the neutral chloride solution and containing different concentrations of Zn_2Al-$EDDS^{4-}$ LDH.

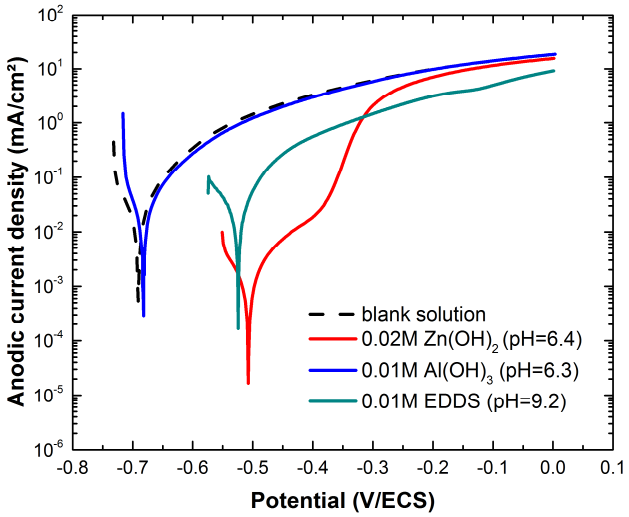

Figure 5: Anodic polarization curves for the carbon steel (RDE rotation speed = 200 rpm) obtained after 24 h in the 0.1M NaCl electrolyte containing the components that are part of the synthetized $Zn_2Al\text{-}EDDS^{4-}$.. The curve in dashed line, obtained in the neutral chloride solution is reported for comparison.

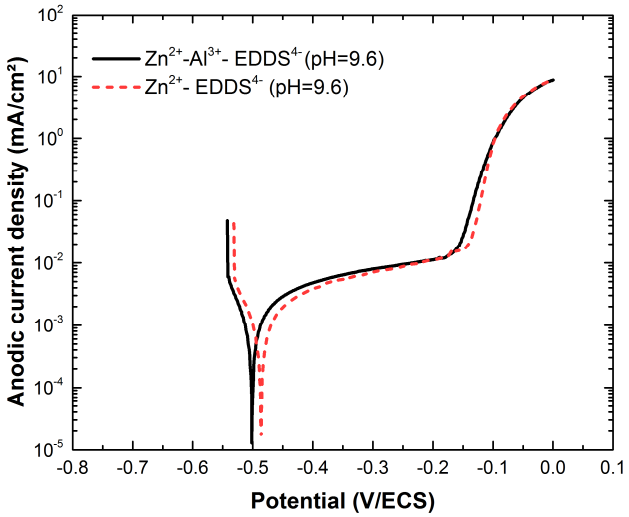

Figure 6: Anodic polarization curves obtained for the carbon steel (RDE rotation speed = 200 rpm) after 24 h of immersion in the solution containing the anion couple Zn^{2+} + $EDDS^{4-}$ and with Al^{3+} cations.

Figure 7 shows the surface states of the carbon steel after 24 h of immersion at corrosion potential in different electrolytes. The LDH-$EDDS^{4-}$ (5 g/L) limits the dissolution of iron by comparison with the sample immersed in the neutral chloride solution (generalized corrosion), but some corrosion defects are visible. When only Zn^{2+} cations are present in the electrolyte, the sample is protected by the formation of some whitish scales-like precipitates at the surface. The corrosion which appears on the surface of the electrode exhibits a spiral form due to hydrodynamics. For EDDS alone in the chloride solution, the surface of the sample is grey with some pits which are not very visible due to complexing effect with Fe(II) or Fe(III). This complexing effect is well equivalent to that of EDTA (Metsärine et al., 2011). However, when the inhibitive components are in mixture, the carbon steel surface is totally protected.

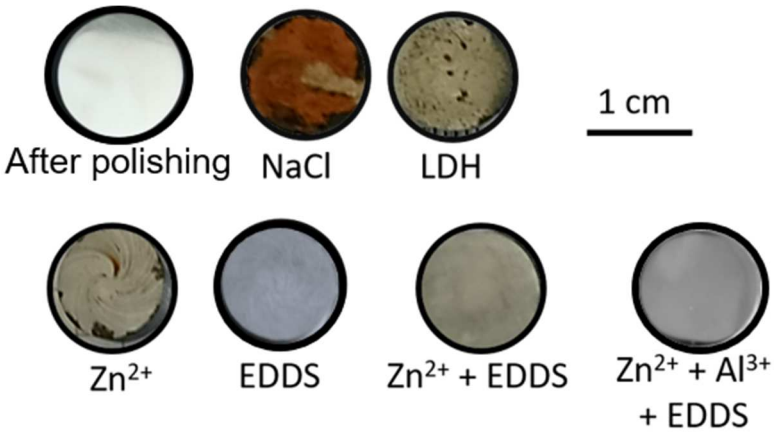

Figure 7: Macrographs of the carbon steel sample exposed during 24 h to the neutral chloride solution (RDE rotation speed = 200 rpm) with the addition of components alone or in mixture.

Electrochemical impedance spectroscopy is carried out to obtain more information about the inhibitive mechanism provided by LDH containing EDDS. Figure 8 shows the impedance diagrams, in Bode coordinates, obtained for the carbon steel after 24h of immersion at corrosion potential in the neutral aerated chloride solution without inhibitive component and the solution containing LDH-$EDDS^{4-}$ components for two different concentrations. For the 0.1 M NaCl electrolyte, the impedance diagram is characterized by one single time constant at around 0.3 Hz, attributed to the charge transfer due to the

dissolution of iron. When LDH-EDDS^{4-} are added in the blank electrolyte, the impedance modulus is higher than without and highest for the more concentrated solution. In parallel, the phase diagram shows a second time constant at higher frequency, which is described in literature as the chelation between ethylenediamine-N,N'-disuccinic acid molecule and divalent metallic iron cation (Jaber et al., 2020). The LDH concentration in the electrolyte is an important parameter because the electrochemical response is different when the concentration is higher, the substrate being more resistive to the corrosion phenomena. This result indicates that the synergy effect between Zn^{2+} and EDDS^{4-} ions depends on the LDH concentration in the electrolyte.

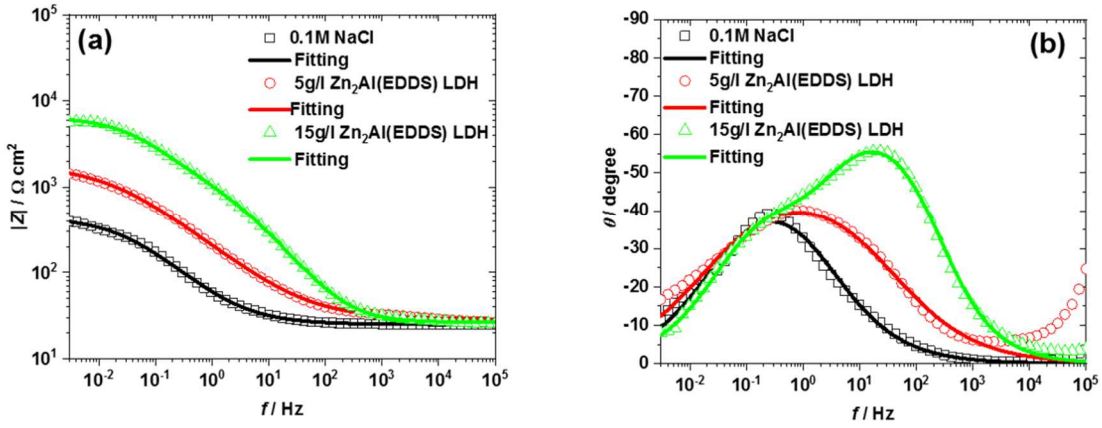

Figure 8: Electrochemical impedance diagrams in Bode coordinates: (a) impedance modulus and (b) phase angle *vs* frequency, obtained at corrosion potential for the carbon steel after 24h of immersion in 0.1M NaCl containing LDH-EDDS^{4-} (RDE rotation speed = 200 rpm). The result obtained without inhibitive components is reported for comparison.

In the same way than the previous result from the potentiodynamic measurements, impedance diagrams are obtained after 24 h of immersion in the chloride solution containing the different components constituting the functionnalized LDH, either alone, or in mixture (Fig. 9). The shape of impedance diagrams is different for the different electrolytes. In presence of zinc, the Bode diagram is characterized by two time constants. By analogy to the previous results, the low frequency time constant can be attributed to the dissolution of iron and the high frequency time constant can be attributed to the

precipitation of Zn^{2+} onto the carbon steel surface as described for the galvanized steel. The corrosion of steel should increase the interfacial pH and promote simonkoellite ($Zn_5(OH)_8Cl_2$-H_2O) precipitation (Too et al., 2014). The impedance diagrams in presence of EDDS alone is characterized by a single time constant at medium frequency. That could be attributed to charge transfer by complexing under the release of divalent or trivalent iron. When the two components are in the electrolyte, the impedance diagram is characterized by two imbricated time constants and the impedance modulus at low frequency is highest. These observations agree with the polarization curves and highlight the beneficial impact of synergistic effect between zinc and EDDS ions. The impedance diagrams are fitted by using electrical equivalent circuit (Fig. 10 a for the one time constant impedance diagrams and Fig. 10 b for two times constants) to extract the kinetic characteristics of the interface metal/electrolyte. The high frequency time constant is attributed to the presence of a film (chelate or pseudo-passivation of iron regarding the case) and the low frequency time constant is attributed to the charge transfer related to iron dissolution. The electrolyte resistance (R_e) and the CPE parameters, α and Q are graphically extracted according to (Orazem et al., 2006), and these values are introduced into the model to guide the fit as hypothesis paramters. The adjustment of the impedance data is performed using a recently available software that employs simplex to fine-tune initial guesses and Levenberg-Marquardt regression to extract parameters (https:///escarxiv.org/kze9x). Table 4 reports the fitted parameters as well as the inhibition efficiency obtained from the equation 5, where $R_{ct,0}$ and $R_{ct,inh}$ are the charge transfer resistances without and with inhibitive component, respectively (Outirite et al., 2010):

$$IE\ (\%) = \frac{R_{ct,inh} - R_{ct,0}}{R_{ct,inh}} \qquad \text{(eq. 5)}$$

The micrographs of the carbon steel surface after 24 h of immersion at corrosion potential in the different electrolytes, obtained by SEM, are presented in Figure 11. The impedance results are discussed regarding to the surface observations.

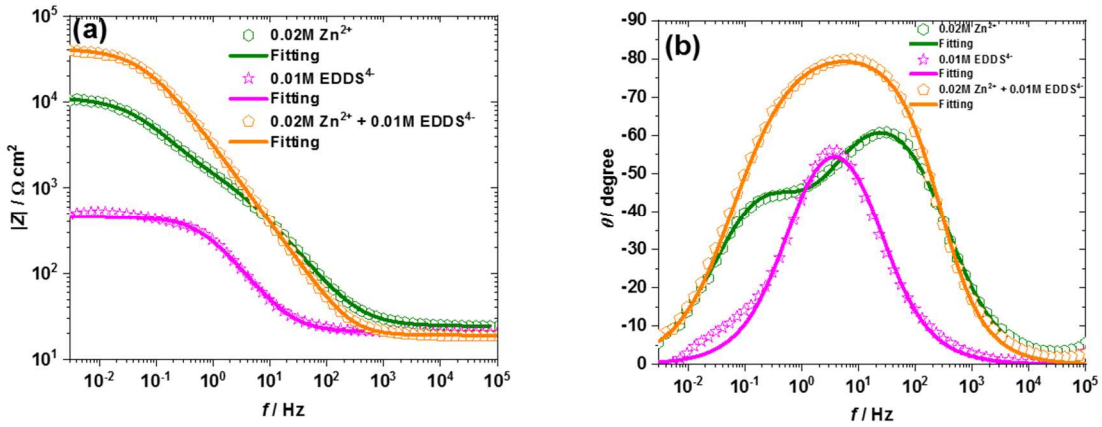

Figure 9: Electrochemical Bode impedance diagrams obtained at corrosion potential for the carbon steel after 24h of immersion in the neutral chloride solution (rotation speed = 200 rpm) containing 0.02M Zn^{2+} or/and 0.01M $EDDS^{4-}$ ions.

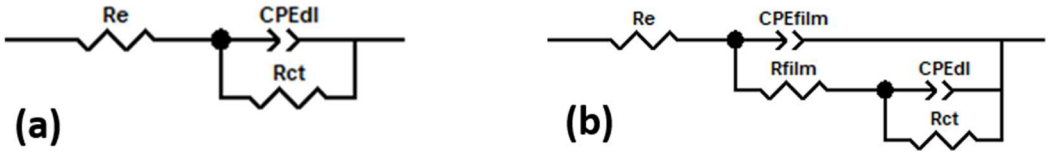

Figure 10: Electrical equivalent circuits used to fit the impedance diagrams characterized by: (a) one single-time constant and (b) two well defined or not well dissociated time constants.

Table 4: Impedance parameters obtained from the fitting procedure using electrical equivalent circuits presented in Figure 10 and the Levenberg-Marquardt regression (https:///escarxiv.org/kze9x).

Electrolyte	Model used	Re / Ω cm²	α_{film}	Q_{film} / Ω^{-1} cm^{-2} s^{a}	R_{film} / Ω cm²	α_{dl}	Q_{dl} / Ω^{-1} cm^{-2} s^{a}	R_{ct} / Ω cm²	IE / %
Blank solution (0.1 M NaCl)	Fig. 10 a	25 ± 0.1	-	-	-	0.63 ± 0.004	7.12 10^{-3} ± 5.8 10^{-5}	418 ± 5	-
Blank + LDH-$EDDS^{4-}$ (5 g/L)	Fig. 10 a	29 ± 0.2	-	-	-	0.55 ± 0.003	1.80 10^{-3} 1.4 10^{-5}	1789 ± 25	77
Blank + LDH-$EDDS^{4-}$ (15 g/L)	Fig. 10 b	27 ± 0.1	0.77 ± 0.004	1.32 10^{-4} ± 3.5 10^{-6}	1223 ± 71	0.62 ± 0.013	3.57 10^{-4} ± 1.0 10^{-5}	5392 ± 127	92
Blank + Zn^{2+}	Fig. 10 b	25 ± 0.1	0.81 ± 0.003	7.79 10^{-5} ± 1.3 10^{-6}	1657 ± 48	0.73 ± 0.008	2.17 10^{-4} ± 2.6 10^{-6}	9707 ± 106	95
Blank + $EDDS^{4-}$	Fig. 10 a	21 ± 0.1				0.84 ± 0.005	7.75 10^{-4} ± 1.5 10^{-5}	473 ± 4	11
Blank + Zn^{2+} + $EDDS^{4-}$	Fig. 10 b	19 ± 0.1	0.91 ± 0.002	5.65 10^{-5} ± 7.3 10^{-7}	20642 ± 2970	0.62 ± 0.063	6.69 10^{-5} ± 2.4 10^{-5}	21568 ± 3450	98

The electrochemical behavior of carbon steel is different when either $Zn(OH)_2$, or EDDS is added to the neutral chloride solution (Fig. 9). In presence of Zn^{2+}, a contribution of the impedance response is due to the presence of a film and the charge transfer resistance is strong (9707 Ω cm^2, Table 4). The SEM micrographs revealed the presence of zinc-based film that should protect the carbon steel surface (Fig. 11 a). The surface condition must be due to the dissolution of iron which induces the interfacial pH to increase and to promote the simonkolleite precipitation (Too et al., 2014). This proposed mechanism is in agreement with the polarization curve in Figure 5. Moreover, the high inhibition efficiency as high as 95 % (Table 4) is explained by the beneficial impact due to the precipitation of Zn^{2+} on the surface as protection of the cut edge of the galvanized steel (Souto et al., 2010).

In the presence of EDDS alone in the 0.1 M NaCl solution, the charge transfer resistance is in the same order of magnitude with that of 0.1 M NaCl electrolyte (around 400-500 Ω cm^2, Table 4). After 24h of immersion with 0.01 M EDDS (pH = 9.2), the carbon steel surface state is characterized by the presence of pits of about 20 µm of diameter and the dissolution of iron cations that further complex with $EDDS^{4-}$ anions (Figs. 11 b and c). The lowest inhibition efficiency equal to 11% determined for this electrolyte is in agreement with the localized corrosion due to the effect of chlorides.

When the Zn^{2+} and $EDDS^{4-}$ are in mixture, the carbon steel surface is fully protected (Fig. 11 c) From the impedance parameters reported in Table 4, the film resistance which is attributed to the pseudo-passivation of iron and the chelate between Fe^{2+} ions and EDDS, is about ten times higher than for the electrolyte containing only Zn^{2+} and the charge transfer resistance is twice higher. The synergy mechanism is due to the adsorption of EDDS together with a modification of the interfacial pH in presence of Zn^{2+}. The inhibition efficiency, reported in Table 4, equal to 98 % is the result of the concomittant effect between both components acting in synergy in terms of their efficiency.

The concentration of LDH-$EDDS^{4-}$ in the electrolyte has a direct effect on the electrochemical behavior of the carbon steel with the appearance of higher impedance modulus (15 g/L). The higher the content in the solution, the higher the exchange between intercalated EDDS and Cl^-. The corrosiveness of solution decreases due the entrapment of chloride by LDH scavenger while the complex formation between $EDDS^{4-}$ anions and Fe^{2+}

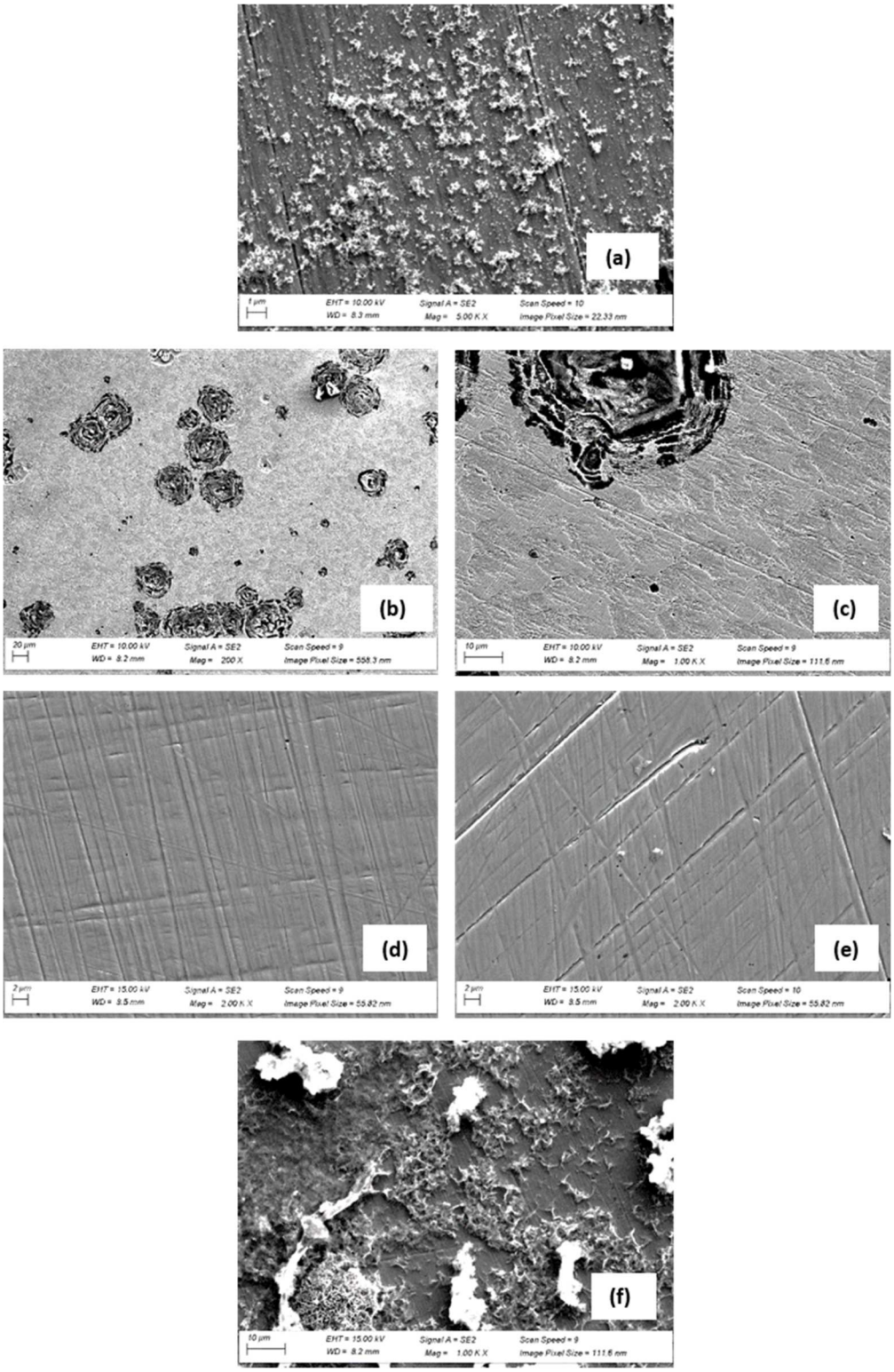

Figure 11: SEM micrographs of the carbon steel after 24 h of immersion in the neutral chloride solution (200 rpm) containing: (a) 0.02 M of $Zn(OH)_2$ (pH = 6.4), (b) and (c) 0.01 M of EDDS at different magnifications (pH = 9.2), (d) 0.02 M of $Zn(OH)_2$ + 0.01 M EDDS (pH = 9.6) and (e) 0.02 M $Zn(OH)_2$ + 0.01 M EDDS + 0.01 M $Al(OH)_3$ (pH = 9.6) and (f) 5 g/L of LDH-$EDDS^{4-}$ (pH = 6.8).

iron cations promote protective film formation thereby enhance corrosion protection. The SEM micrograph obtained for a protected surface at the lower concentration of hybrid LDH (5 g/L) (Fig. 11 f) shows two types of surface state most presumably coming from Zn^{2+}-based films and the formation of complexes between EDDS molecules and the cations Fe^{2+}. In comparison to Fig 11a, the spider web shaped network must come from Zn-based films while coarser, whiter (under electron beam so more insulating) lumps seem to come from EDDS(Fe) complexes. From the impedance diagrams (Fig. 8) and the associated refined parameters (Table 4), it clearly shows that the efficiency of the synthetized LDH-$EDDS^{4-}$ is depending on the concentration of loaded LDH.

The inhibition mechanism from LDH-$EDDS^{4-}$ can be explained by:

(i) LDH-EDDS promotes the decrease of the corrosiveness of the electrolyte by exchange between Cl^- and $EDDS^{4-}$ out of the LDH cargo,

(ii) the release of EDDS induces corrosion inhibition by a complexing effect with Fe^{2+}, while such increase in anodic dissolution induces an increase in zinc (II) reduction which should modify the interfacial pH.

(iii) These phenomena promote the precipitation of the simonkoellite or LDH on the surface, and the adhesion of the corrosion products should be due to the mixture between Fe(II) or Fe(III)-EDDS complex and LDH or simonkoellite, surface analysis are in progress to validate this assumption.

4. Conclusion

This work focuses on understanding the mechanism of inhibition of carbon steel in presence of a host/guest-based inhibitor. Selected hybrid $[Zn_2Al(OH)_6]^+[EDDS^{4-}]_{0.25}.2H_2O$ LDH is found to inhibit effectively exhibit corrosion protection that is not only due to anion-exchange mechanism but also a partial and rather selective solubility of the LDH scaffold leading to the presence of zinc in solution. A synergy effect between zinc hydroxide and EDDS is clearly identified. From the electrochemical results some important points can be sumarized below:

- trapping effect of chloride by anion exchange with intercalated EDDS in the LDH cargo inducing a decreasing of agressivess of the electrolyte,

- releasing of both $EDDS^{4-}$ and Zn^{2+} ions from LDH scaffold due to its partial solubility,

- synergy effect between $EDDS^{4-}$ and Zn^{2+} explained by a competitive effect between the adsorption of EDDS and the buffering effect from the Zn^{2+} precipitation on carbon steel surface,

- Al^{3+} has no role in inhibiting corrosion of carbon steel .

The synergy effect is still under study to demonstrate the interest to elaborate a smart coating loaded with this type of particles where a particular attention will be paid to the interaction between the LDH and the organic matrix.

Acknowledgements: The authors would like to thank the Petroleum Technology Development Fund (Nigeria) for the financing of the Gata Joseph Ayemi PhD.

References

Alibakhshi E., Ghasemi E., Mahdavian M., Ramezanzadeh B., Farashi S., 2017. Active corrosion protection of Mg-Al-PO 4 3− LDH nanoparticle in silane primer coated with epoxy on mild steel. Journal of the Taiwan Institute of Chemical Engineers 75, 248-262.

Alibakhshi E., Ghasemi E., Mahdavian M., Ramezanzadeh B., Yasaei M., 2020. The effect of interlayer spacing on the inhibitor release capability of layered double hydroxide based nanocontainers. Journal of Cleaner Production 251, 119676.

Bakhtaoui N., Benali O., Mazarío E., Recio F. J., Harrasti P., 2021. Layered double hydroxides intercalated with methyl orange as a controlled-release corrosion inhibitor for iron in chloride media. Nano Express 2, 010017.

Cao Y., Dong S., Zheng D., Wang J., Zhang X., Du R., Song G., Lin C., 2017. Multifunctional inhibition based on layered double hydroxides to comprehensively control corrosion of carbon steel in concrete. Corroion Science 126, 166-179.

Cao, Y., Zheng, D., Lin, C., 2021. Effect of physical barrier and anion-exchange process of nitrate-intercalated ZnAl layered double hydroxide films grown on Al on corrosion protection. Surface and Coatings Technology 421, 127436.

Cao Y., Zheng D., Zhang F., Pan J., Lin C., 2022. Layered double hydroxide (LDH) for multi-functionalized corrosion protection of metals: A review. Journal of. Materials Science and Technology 102, 232-263.

Chhetri S., Samanta P., Murmu N., Kuila T., 2019. Anticorrosion Properties of Epoxy Composite Coating Reinforced by Molybdate-Intercalated Functionalized Layered Double Hydroxide. Journal of Composites Science 3, 11.

Deip A.R., Leal D.A., Sakae G.H., Maia F., Berton M.A.C., Ferreira M.G.S., Marino C.E.B., 2020. Performance of commercial LDH traps for chloride ion in a commercial corrosion protection primer for petrochemical industry. Corrosion Engineering Science and Technology 55, 66-74.

Ekott E.J., Akpabio E.J., Etukudo U.I., 2012. Cathodic Protection of Buried Steel Oil Pipelines in Niger Delta, Environmental Research Journal 6, 304-307.

Ennadi A., Legrouri A., De Roy A., Besse J.P., 2000. X-Ray Diffraction Pattern Simulation for Thermally Treated [Zn–Al–Cl] Layered Double Hydroxide., Journal of Solid State Chemistry 152, 568-572.

Garden L., Pethrick R.A., 2017. A dielectric study of water uptake in epoxy resin systems, Journal of Applied Polymer Science 134, 44717.

Hang T.T.X., Duong N.T., Truc T.A., Hoang T., Thanh D.T.M., Daopiset S., Boonplean A., 2015. Effects of hydrotalcite intercalated with corrosion inhibitor on cathodic disbonding of epoxy coatings. Journal of Coatings Technology Research 12, 375-383.

Hang T.T.X., Truc T.A., Duong N.T., Vu P.G., Hoang T., 2012. Preparation and characterization of nanocontainers of corrosion inhibitor based on layered double hydroxides. Applied Clay Science 67–68, 18-25.

Jaber S., Leremboure M., Thery V., Delort A.-M., Mailhot G., 2020. Mechanism of photochemical degradation of Fe(III)-EDDS complex. Journal of Photochemistry and Photobiology A: Chemistry 399, 112646.

Leal D. A., Wypych F., Bruno Marino C.E., 2020. Zinc-Layered Hydroxide Salt Intercalated with Molybdate Anions as a New Smart Nanocontainer for Active Corrosion Protection of Carbon Steel. ACS Applied Materials & Interfaces 12, 19823-19833.

Li W., Liu A., Tian H., Wang D., 2018. Controlled Release of Nitrate and Molybdate Intercalated in Zn-Al-Layered Double Hydroxide Nanocontainers towards Marine Anticorrosion Applications. Colloids and Interface Science Communications 24, 18-23.

Liu J., Shi H., Yu M., Du R., Rong G., Li S., 2019. Effect of divalent metal ions on durability and anticorrosion performance of layered double hydroxides on anodized 2A12 aluminum alloy. Surface and Coatings Technology 373, 56-64.

Mei Y., Xu J., Jiang L., Tan Q., 2019. Enhancing corrosion resistance of epoxy coating on steel reinforcement by aminobenzoate intercalated layered double hydroxides. Progress in Organic Coatings 134, 288-296.

Metsärine S., Tuhkanen T., Aksela R., 2011. Photodegradation of ethylenediaminetetraacetic acid (EDTA) and ethylenediamine disuccinic acid (EDDS) within natural UV rafdiation range. Chemosphere 45, 949-955.

Morsch S., Lyon S., Greensmith P., Smith S.D., Gibbon S.R., 2015. Mapping water uptake in organic coatings using AFM-IR. Faraday Discussions 180, 527-542.

Nguyen D.T., To H.T.X., Gervasi J., Paint Y., Gonon M., Olivier M.-G., 2018. Corrosion inhibition of carbon steel by hydrotalcites modified with different organic carboxylic acids for organic coatings. Progress in Organic Coatings 124, 256-266.

Nguyen Thuy D., To Thi Xuan H., Nicolay A., Paint Y., Olivier M.-G., 2016. Corrosion protection of carbon steel by solvent free epoxy coating containing hydrotalcites intercalated with different organic corrosion inhibitors. Progress in Organic Coatings 101, 331-341.

Obot O.W., Anyakwo C.N., 2017. An Investigation of Internal Corrosion of Oil and Gas Transporting Carbon Steel Pipes in the Niger Delta Area of Nigeria. EJERS 2, 22-26.

Orazem M.E., Pébère N., Tribollet B., 2006. Enhanced Graphical Representation of Electrochemical Impedance Data. Journal of the Electrochemical Society 153, B129.

Outirite M., Lagrenée M., Lebrini M., Traisnel M., Jama C., Vezin H., Bentiss F., 2010. Ac impedance, X-ray photoelectron spectroscopy and density functional theory studies of 3,5-bis(n-pyridyl)-1,2,4-oxadiazoles as efficient corrosion inhibitors for carbon steel surface in hydrochloric acid solution. Electrochimica Acta 55, 1670-1681.

Panda H.S., Srivastava R., Bahadur D., 2011. Synthesis and in situ mechanism of nuclei growth of layered double hydroxides. Bulletin of Materials Science 34, 1599-1604.

Peng G., Qiao Q., Huang K., Wu J., Wang Y., Fu X., Zhang Z., Fang T., Zhang B., Huang Y., Li X., 2020. Ni-Fe-MoO42- LDHs/epoxy resin varnish: A composite coating on carbon steel for long-time and active corrosion protection. Progress in Organic Coatings 140, 105514.

Rodriguez J., Bollen E., Nguyen T.D., Portier A., Paint Y., Olivier M.-G., 2020. Incorporation of layered double hydroxides modified with benzotriazole into an epoxy resin for the corrosion protection of Zn-Mg coated steel. Progress in Organic Coatings 149, 105894.

Seniski A., Monteiro R.F., Carrera G.T, d'Orey M., Bragança G.P., Portella K.F., 2020. The inhibitory and comparative effects of Zn-Al layered double hydroxide microcontainers intercalated with benzotriazole and nitrite for corrosion protection coatings on AISI 1010 carbon steel. Matéria (Rio de Janeiro) 25.

Serdechnova M., Salak A.N., Barbosa F.S., Vieira D.E.L., Tedim J., Zheludkevich M.L., Ferreira M.G.S., 2016. Interlayer intercalation and arrangement of 2-mercaptobenzothiazolate and 1,2,3-benzotriazolate anions in layered double hydroxides: In situ X-ray diffraction study. Journal of Solid State Chemistry 233, 158-165.

Souto R. M., Normand B., Takenouti H., Keddam M., 2010. Self-healing processes in coil-coated cladding studied by the canning vibrating electrode. Electrochimica Acta 55, 4551-4457.

Stimpfling T., Leroux F., Hintze-Bruening H., 2012. Phosphate-Based Organic Molecules Interleaved with Layered Double Hydroxide: Unraveling the Roles of Host Cations and the Guest-Inhibiting Effect in Aluminum Corrosion Protection. European Journal of Inorganic Chemistry 5396-5404.

Stimpfling T., Leroux F., Hintze-Bruening H., 2013. Unraveling EDTA corrosion inhibition when interleaved into Layered Double Hydroxide epoxy filler system coated onto aluminum AA 2024. Applied Clay Science 83-84, 32-41.

Theiss F.L., Ayoko G.A., Frost R.L., 2016. Synthesis of layered double hydroxides containing Mg^{2+}, Zn^{2+}, Ca^{2+} and Al^{3+} layer cations by co-precipitation methods-A review. Applied Surface Science 383, 200-213.

Too J. D., Ogle K., Volovitch P., 2014. The effect of synthetic zinc corrosion products on corrosion of electrogalvanized steel. II. Zinc reactivity and galvanic coupling zinc/steel in presence of zinc corrosion products. Corrosion Science 83, 32-37.

Truc T.A., Thuy T.T., Oanh V.K., Hang T.T.X., Nguyen A.S., Caussé N., Pébère N., 2019. 8-hydroxyquinoline-modified clay incorporated in an epoxy coating for the corrosion protection of carbon steel. Surfaces and Interfaces 14, 26-33.

Wang Y., Zhang D., 2011. Synthesis, characterization, and controlled release anticorrosion behavior of benzoate intercalated Zn–Al layered double hydroxides. Materials Research Bulletin 46, 1963-1968.

Zhang D., Zhang H., Zhao S., Li Z., Hou S., 2019. Electrochemical Impedance Spectroscopy Evaluation of Corrosion Protection of X65 Carbon Steel by Halloysite Nanotube-Filled Epoxy Composite Coatings in 3.5% NaCl Solution. International Journal of Electrochemical Science 14, 4659-4667.

Zheludkevich M.L., Tedim J., Ferreira M.G.S., 2012. “Smart” coatings for active corrosion protection based on multi-functional micro and nanocontainers. Electrochimica Acta 82, 314-323.

Zhou M., Yan L., Ling H., Diao Y., Pang X., Wang Y., Gao K., 2017. Design and fabrication of enhanced corrosion resistance Zn-Al layered double hydroxides films based anion-exchange mechanism on magnesium alloys. Applied Surface Science 404, 246-253.